LBL-18117
Preprint c.2

Lawrence Berkeley Laboratory

UNIVERSITY OF CALIFORNIA

RECEIVED
LAWRENCE
BERKELEY LABORATORY

SEP 10 1984

LIBRARY AND
DOCUMENTS SECTION

Submitted to Physics in Medicine and Biology

DEAD TIME CORRECTION AND COUNTING STATISTICS
FOR POSITRON TOMOGRAPHY

B.M. Mazoyer, M.S. Roos, and R.H. Huesman

July 1984

TWO-WEEK LOAN COPY
This is a Library Circulating Copy
which may be borrowed for two weeks

Donner

Biology & Medicine Division

LBL-18117 c.2

Prepared for the U.S. Department of Energy under Contract DE-AC03-76SF00098

DISCLAIMER

This document was prepared as an account of work sponsored by the United States Government. While this document is believed to contain correct information, neither the United States Government nor any agency thereof, nor the Regents of the University of California, nor any of their employees, makes any warranty, express or implied, or assumes any legal responsibility for the accuracy, completeness, or usefulness of any information, apparatus, product, or process disclosed, or represents that its use would not infringe privately owned rights. Reference herein to any specific commercial product, process, or service by its trade name, trademark, manufacturer, or otherwise, does not necessarily constitute or imply its endorsement, recommendation, or favoring by the United States Government or any agency thereof, or the Regents of the University of California. The views and opinions of authors expressed herein do not necessarily state or reflect those of the United States Government or any agency thereof or the Regents of the University of California.

Dead Time Correction and Counting Statistics for Positron Tomography

B. M. Mazoyer, M. S. Roos and R. H. Huesman

Donner Laboratory and Lawrence Berkeley Laboratory,

University of California, Berkeley, California 94720

LBL-18117

submitted to Physics in Medicine and Biology

Abstract

A correction for loss of events due to dead time in dynamic positron emission tomography is presented. The model employs a paralyzing dead time to describe the behavior of the tomograph over the range of event rates normally encountered in patient studies (up to 200,000 events/sec/detector layer). The Donner 280-Crystal Positron Tomograph is characterized by a dead time of 1.8 μsec/event for observed count rates of less than 200,000 events/sec. The dead time correction factor is 1.8 at 180,000 events/sec. The correction is applied to projection data and to region of interest analysis of dynamic PET studies, and the covariances of the corrected data are calculated. At 180,000 events/sec, the variance of the actual (corrected) number of events in a region containing 3.3×10^5 actual events is predicted from the model to be 3.9×10^6 events^2, which is more than 10 times the variance that would be expected from a naive assumption of Poisson statistics. These statistical results are verified experimentally. The necessity and importance of dead time correction in dynamic PET is shown by an example of an observed error of 25% in myocardial flow if dead time compensation is not applied.

Introduction

A correction for dead time is necessary for quantitative positron emission tomography, in addition to the corrections for attenuation and detector sensitivity. All these corrections are applied to emission data in which each bin corresponds to a chord between two crystals in a circular detector array. The corrected number of events in the kth bin, p_k, depends on two observations: an emission dataset acquired after a positron emitting radionuclide has been introduced and a transmission dataset acquired previous to injection and used for attenuation correction. In the transmission experiment an annular source of ^{68}Ge surrounds the patient port and data are taken with the patient in position, in analogy to X-ray CT. Both datasets are subject to the effect of dead time, so that the number of events detected in a time interval is a nonlinear function of the activity in the tomograph. In addition, each of these datasets has associated uncertainties that must be accounted for throughout the analysis in order to estimate the variance of the result.

Defining $q^e{}_k$ and $q^t{}_k$ as the emission and transmission datasets, the corrected number of events is given by

$$p_k = f^e q^e_k \frac{T^t}{f^t q^t_k} H_k \quad , \tag{1}$$

where T^t is the acquisition period of the transmission data. The dead time correction factors for the emission and transmission files are f^e and f^t. H_k denotes theoretical unit duration transmission data with the tomograph empty and incorporates the correction for detector efficiency and geometry.

The H_k are determined empirically through phantom studies but with such precision that they are taken to be non random parameters in the analysis below.

In section 1, the dead time correction problem is approached by constructing a simple model of the dead time behavior of the positron tomograph, assuming that it may be paralyzed and can be described in a limited range of count rates by a single dead time. No attempt is made to model the event processing logic of the tomograph, which is described elsewhere (Derenzo et al 1981, Huesman et al 1980). The parameters of the model are determined through experiments with a short-lived positron emitter, ^{82}Rb. In section 2, we derive estimates of variance for histogrammed data and regions of interest. Results of both sections are validated by another experiment in which we sample the statistics of the events detected by the tomograph at a wide range of count rates using ^{18}F and measure the dead time correction factor directly using ^{68}Ge. This method is similar to that proposed for dead time correction in Anger cameras (Adams et al 1973, Budinger et al 1973). An application to dynamic PET flow studies demonstrating the importance of the dead time correction appears in section 3.

Section 1: Dead time correction

Model for events

The positron tomograph detects an event when photons strike two detectors, producing electrical pulses of the appropriate energy within a fixed coincidence window. Events involving two photons are due either to the annihilation of one positron with both photons detected (called actual

events here) or to one photons from each of two annihilations (called accidentals). The total numbers of actual and accidental events that would be recorded in an interval in the absence of dead time are denoted A and B, respectively. Events involving three or more photons, triples, result from the annihilation of at least two positrons and are rejected by the electronics.

In order to determine the dead time of the tomograph, one can observe the decay of a source. The total number of events in equal time intervals of duration T from a positron emitter placed in the tomograph behave approximately according to:

$$\begin{aligned} A(i) &= \alpha_1 \exp(-\lambda t_i) \\ B(i) &= \beta_1 \exp(-2\lambda t_i) \quad , \end{aligned} \tag{2}$$

where λ is the decay constant of the positron emitter, t_i is the time at the center of the ith interval, and α_1 and β_1 are the number of actual and accidental events in the first interval. It is assumed that the duration of the intervals is small compared with the half-life of the positron emitter. Notice that A(i), the number of actual events, is proportional to activity in the tomograph while B(i), the number of accidental events, is proportional to activity squared.

The Donner 280-Crystal Positron Tomograph employs a ^{68}Ge hoop source for transmission studies. When the hoop is retracted into a groove in the collimator for emission studies, its scattered photon emissions appear to the detectors as a source of single photons. A few true coincident events due to the hoop are also detected because the metal cover on the hoop is not thick enough to stop all positrons. There are also a small number of events due to background radiation. The relations above may be easily

modified to account for the presence of long-lived emitters:

$$A(i) = \alpha_1 \exp(-\lambda t_i) + \alpha_2$$
$$B(i) = \beta_1 \exp(-2\lambda t_i) + \beta_2 \exp(-\lambda t_i) + \beta_3 \ . \qquad (3)$$

Here α_2 is the number of actual events due to a long-lived positron emitter, β_3 is the number of accidental coincidences due to a long-lived radionuclide, and β_2 represents events with one photon from the short-lived positron emitter and one from the long-lived radionuclide.

The total number of events in coincidence in an interval is A+B (where (i) has been dropped). In order to estimate A an estimate of B is subtracted from the total. The estimate of B is obtained with a second coincidence window of equal duration but with a sufficient time delay inserted on one input channel so that only accidentals are detected. The first coincidence window will be referred to as the on-time window and the second as the off-time window.

Model for losses due to dead time

In our simple model, the dead time processes are lumped into a single paralyzing dead time τ (see for example Evans 1955), simply described by:

$$\text{observed rate} = \text{rate} \times \exp(-\ \tau \times \text{rate}\ ) \qquad (4)$$

Events from both the on-time and off-time windows generate the same dead time, thus the number of events lost due to dead time will be determined by the total event rate (A+2B)/T . If N is the number of observed on-time events and M is the number of observed off-time events, then

$$N = \frac{A + B}{f}$$
$$M = \frac{B}{f} \quad , \tag{5}$$

where f is the dead time correction factor given by

$$f = \exp[\ \tau \frac{(A + 2B)}{T}\ ] \quad , \tag{6}$$

and 1 - 1/f is the fraction of events lost due to dead time.

Figure 1 shows data acquired with ^{82}Rb in the Donner 280-Crystal Positron Tomograph. Notice that in order to correct data an estimate of the real count rate, (A+2B)/T, must be calculated using the total observed count rate (N+M)/T and equation (4). This nonlinear equation is solved using Newton's method, with the range restricted a priori to values less than the maximum observed (N+M)/T.

Estimation of dead time

To obtain a dataset from which τ could be determined, 40 ml of saline solution containing 50 mCi of ^{82}Rb were injected into a vial placed in the sensitive plane of the tomograph. N and M were recorded for 80 sequential intervals of 10 sec. The data are plotted in figure 1a. It is not obvious that the entire dataset can be characterized by a model based on only one paralyzing dead time. In practice our interest is restricted to the lower range of count rates and we assume that other dead times are too short to induce losses in this range. Unless specified otherwise the discussion below will pertain to this subset of the data, which appears to the right of the peak in N+M (see figure 1).

It was anticipated that the dead time might be sensitive to the fraction of accidentals, not accounted for in the model. The fraction of

accidentals becomes larger when many scattered photons reach the detectors. These photons may change the effective dead time of the circuits used for pulse height selection for each crystal (Arnold et al 1974, Muehllehner et al 1974). In order to test this hypothesis, the experiment was repeated with the vial immersed in a beaker of water so that the path of each photon traversed approximately 10 cm of water, resulting in significantly higher accidental rates. These data are displayed in figure 1b.

The data for the fit were the recorded quantities N and M with count rates (N+M)/T between 10,000 and 200,000 counts/sec. The decay constant of ^{82}Rb was fixed corresponding to a 75 sec half-life, and the parameters α_1, α_2, β_1, β_2, β_3, and τ were estimated to fit equation (3), (5) and (6) using a weighted least-squares criterion and a Marquardt-type algorithm (Marquardt 1963). In order to test the validity of our model, another set of data recorded at low event rates was also fit. The observed values of N and M were used as estimates of variance of these variables for the weighted least-squares fits.

The results of these fits are summarized in figure 2. The dead time estimates were 1.789 ± 0.006 μsec/event for the vial only and 1.819 ± 0.006 μsec/event with the water phantom. The dead time correction thus depends on the accidental rate, but the effect is small compared to the correction itself. The dead time correction factors obtained by using these two values are very close as can be seen in figure 3a.

Validity of the model

In order to test the validity of the model the following experiment was performed: A source containing ≈ 28 μCi ^{68}Ge (half-life 282 days) and a

source ≈ 59 mCi ^{18}Fluoro-deoxy-glucose in 29 ml water (half-life 110 min) were placed in the tomograph. A series of 80 files (1 sec each) was collected every half hour for 24 hours. Datasets for attenuation correction were also taken with each of the vials replaced by a lucite phantom. Regions of interest including each source were drawn on a reconstructed image (figure 4), and the total number of events in each region was computed for each series of 80 files (Huesman 1984). By looking at the events at the ^{68}Ge location we were able to estimate an experimental correction factor for different total count rates, neglecting the ^{68}Ge decay during the 24 hour experiment. Neglecting the decay of the ^{18}FDG during each series of 80 files, experimental values for the covariance of N and M were calculated.

The dead time correction factor determined from the ^{68}Ge region agrees closely with that obtained from the model using τ = 1.8 μsec/event (figure 3b) in the range of count rates included in the scope of this study. Fitting the ^{68}Ge-^{18}FDG dataset with the model gives a value of 1.794 ± 0.014 μsec/event, not significantly different from the values obtained with the ^{82}Rb datasets.

Discussion

The model of event handling in the tomograph does not explicitly include three photon events, or triples, as do other previously published models (Hoffman et al 1983). These events are rejected by the tomograph but still contribute dead time. This is absorbed by τ, which is really an effective dead time. Because the triples rate is not expected to be proportional to the total event rate some model error is introduced. Based on the experiments described above and a coincidence window of 25 nsec, the

triples rate can be predicted. We consider two types of triples: those involving two annihilation events which occur at a rate equal to the product of the window duration, the actual events rate and the singles rate; and those involving three annihilation events, whose rate is the product of the window duration, the accidentals rate and the singles rate. We neglect the small number of annihilation events which yield three photons. The triples rate for the ^{82}Rb study with scattering at an observed total count rate of 200,000 events/sec is estimated at 20,000 events/sec, while the actual and accidental rates are 100,000 events/sec and 150,000 events/sec, respectively. Thus triples are about 5 percent of the two photon rate (actual + 2 accidental) at the highest count rate considered, and it is not unreasonable to neglect them.

Another type of event rejected by the tomograph is that in which the photons scatter from one crystal into its neighbor, resulting in pulses from both photomultipliers. Both actual and accidental events are equally likely to be rejected in this way, so that these events merely contribute to the effective τ.

To test the validity of using a single paralyzing dead time to correct in this range, we constructed a model with a paralyzing dead time cascaded with a nonparalyzing dead time. Fitting this model to the dataset with count rates less than 200,000 events/sec yielded a nonparalyzing dead time less than 1 nsec/event, which is not significant. This reflects the exclusion of very high count rates, which makes the two models very similar (Sorenson 1975).

We limit the range of count rates to less than 200,000 events/sec for three reasons: higher count rates have not been encountered often in human or animal studies; the variance of the corrected data can become very large

at high count rates (see Section 2); and while the tomograph exhibits paralyzing behavior, it does not follow a single dead time model beyond the peak in the observed events vs. actual events curve. A multiple dead time model that yielded stable parameter values when fit to different datasets was not found.

Section 2: Variance propagation formula for dead time correction

Preliminaries

In this Section, the dead time correction scheme is applied to transmission and emission data to produce a dataset corrected for detector sensitivity, attenuation and dead time. Recall that the model of Section 1 assumes that the number of events lost due to dead time depends only on the total count rate A+2B and that p_k, the overall corrected value in the kth bin, is defined as:

$$p_k = f^e q_k^e \frac{T^t}{f^t q_k^t} H_k \quad . \tag{1}$$

The superscripts t and e denote transmission and emission datasets, respectively. Since the Donner tomograph substracts accidentals as they occur, the observed quantities are

$$q_k^x = [n_k^x - m_k^x] \quad , \tag{7}$$

where $n^x{}_k$ and $m^x{}_k$ are on-time and off-time events in the kth bin respectively.

The individual $n^x{}_k$ and $m^x{}_k$'s are not observed in the Donner tomograph, but their sums over k, N^x and M^x are counted. Variance estimates from the ^{68}Ge-^{18}FDG experiment discussed in Section 1 are shown in figure 5. The

results suggest that it is reasonable empirically to assume a Poisson distribution for the sums over all bins for total event rates less than 200,000 events/sec. Estimates of the covariance of N^e and M^e, computed for the Ge-FDG experiment, confirm the assumption of independence between these two variables. We make the additional assumption that the individual bin values are independent and Poisson distributed in this range of event rates.

Variances and covariances of p_k's

Equation (1) states that p_k is a function of all of the n^x_k and m^x_k through the dead time correction factors f^x. To estimate the covariance of p_j and p_k, expand to first order:

$$p_j = p_{jo} + \sum_x \sum_i \frac{\partial p_j}{\partial n^x_i} (n^x_i - E(n^x_i)) + \frac{\partial p_j}{\partial m^x_i} (m^x_i - E(m^x_i)) \quad , \tag{8}$$

where E(x) denotes the expectation value of a random variable, and p_{jo} denotes p_j evaluated with the mean values of n^x_i and m^x_i, respectively. By definition,

$$\mathrm{cov}(p_j, p_k) = E(p_j p_k) - E(p_j)E(p_k) \quad , \tag{9}$$

so that to first order:

$$\mathrm{cov}(p_j, p_k) = \sum_x \sum_i \frac{\partial p_j}{\partial n^x_i} \frac{\partial p_k}{\partial n^x_i} \mathrm{var}(n^x_i) + \frac{\partial p_j}{\partial m^x_i} \frac{\partial p_k}{\partial m^x_i} \mathrm{var}(m^x_i) \quad . \tag{10}$$

Equation (10) may be written:

$$\mathrm{cov}(p_j, p_k) = p_j p_k [\, P + \delta_{j,k} Q_k \,] \quad , \tag{11}$$

where

$$P = \sum_x \frac{2f^x f^{x\prime} + (f^{x\prime})^2 (N^x + M^x)}{(f^x)^2} = \sum_x F^x \quad ,$$

and

$$Q_k = \sum_x \frac{n_k^x + m_k^x}{(q_k^x)^2} = \sum_x Q_k^x \ . \tag{12}$$

See Appendix 1 for evaluation of the derivatives in equation (9) and the derivation of equations (11) and (12).

Variance and covariance estimates for counts in regions of interest (ROI)

The correlation among data in different projection bins introduced by dead time correction propagates through region-of-interest calculations and contributes correlation among regions in addition to that which is intrinsic due to reconstruction. Let R^a and R^b be the number of corrected events in two regions of interest. The covariance between R^a and R^b can be estimated by:

$$\mathrm{cov}(R^a,R^b) = \sum_j \sum_k \mathrm{cov}(p_j,p_k)\ c_j^a\ c_k^b \quad , \tag{13}$$

where $c^x{}_j$ are coefficients depending only on the shape of the region and the reconstruction algorithm (Huesman 1984). Using equation (11),

$$\mathrm{cov}(R^a,R^b) = P\ (\sum_j c_j^a\ p_j)(\sum_k c_k^b\ p_k) + \sum_i c_i^a\ c_i^b\ Q_i\ p_i^2 \ . \tag{14}$$

This equation can be rewritten as

$$\mathrm{cov}(R^a,R^b) = f_c^2\ (Pr^a r^b + \mathrm{cov}(r^a,r^b)) \quad , \tag{15}$$

where f_c is the compound correction factor f^e/f^t, r^a and r^b are the uncorrected value in the regions, and the covariance in the brackets the covariance between these uncorrected values (Huesman 1984). Note that the

corrected covariance is not f_c^2 times the uncorrected one, rather there exists an additional term $f_c^2 p_r a_r b$ to account for correlation between f_c and the number of counts in these regions.

Covariance between regions with two different emission datasets

In dynamic studies, a sequence of emission datasets at the same location are acquired and analyzed. Correction of these emission data with a common transmission dataset introduces some correlation between the corrected emission data. It is useful to know this correlation for input to the algorithms used to fit the dynamic data to compartment models.

Calculation of the covariance (or correlation) between bins and regions is a simple extension of equations (11) and (15). Superscripts u and v denote that the data may be from different emission datasets. Then

$$\mathrm{cov}(p_j^u, p_k^v) = p_j^u p_k^v \left(P^* + \delta_{j,k} Q_k^* \right) \quad , \tag{16}$$

where

$$P^* = F^t + \delta_{u,v} F^e \quad ,$$

and

$$Q_k^* = Q_k^t + \delta_{u,v} Q_k^e \ . \tag{17}$$

The covariance between regions is

$$\mathrm{cov}(R^{a,u}, R^{b,v}) = P^* R^{a,u} R^{b,v} + \Sigma_i \left[c_i^a c_i^b Q_i^* p_i^u p_i^v \right] . \tag{18}$$

Validity of covariance propagation formula

The validity of the variance estimates for the sum of events in all bins and for regions was assessed using data from the ^{68}Ge-^{18}FDG experiment (Section 1).

Since computation of the total number of actual events, A, involves only the sums of on- and off-time events without any transmission data, equation (16) may be used to calculate an estimate of the variance of A. For comparison, 80 values of A at the same total count rate are estimated from our experiment, and from these a sample variance is computed. Close agreement between the sample variance and the prediction is demonstrated over a wide range of count rates in figure 6a. It is of interest to note that the coefficient of variation of A, plotted in figure 6b, has a minimum when the count rate is near 100,000 events/sec. Additional activity in the tomograph decreases the precision to which A is determined by a measurement. Analysis of this type can be extended to events within a region of interest in order to determine the optimum dose for a particular experiment.

The estimates of the variance in a region (equation (15)) and the covariance between two regions were tested in a similar manner. In these cases the same transmission file was used so that variability due to the transmission correction could not be observed in the sample. Consequentially, the transmission variance was set to zero in calculation of Q_k. Since $n^e{}_k - m^e{}_k$ is recorded by the tomograph while $n^e{}_k + m^e{}_k$ is required for evaluation of $Q^e{}_k$, we assume that off-time events are uniformly distributed among N_{bin} bins,

$$\hat{m}^e_k = M^e/N_{bin} \quad , \tag{19}$$

so that an estimate of N+M can be calculated. Comparisons between predicted and sample variances are shown in figure 7 and again show good agreement. Covariances between regions are listed in table 1, where covariance estimates without dead time correction are included for comparison.

Note the relative sizes of the contributions of the first and second terms of equation (15) to the covariance. The second term is simply the multiplicative effect of the correction factor on the uncorrected covariance matrix, while the first term reflects the correlation introduced by the correction process. Table 2 shows the contributions to the variance for a background region, the ^{68}Ge region and the ^{18}FDG region for the experiment described above. It is evident that for regions with a large proportion of the total events, e.g. the ^{18}FDG region, that the first term is significant even at low count rates.

Section 3: Application to flow computation

A dead time correction was applied to ^{15}O water flow studies on dogs using a dead time of 1.80 μsec/event. A region of interest in the left ventricle is used to obtain an input function to determine flow into regions in the myocardium (Budinger et al 1984). The input function and residue in the myocardium are shown in figure 8. Comparison of the raw and dead time corrected curves shows that large corrections are necessary when the bolus of radionuclide passes through the heart. Fitting raw and dead time corrected data to a two compartment model yields flows of 1.83 ± 0.17 and 1.39 ± 0.12 ml/min/g, respectively. The flow value determined from the microspheres reference organ technique was 1.47 ml/min/g. Dead time correction decreased the flow value relative to that obtained with raw data in all of twelve dogs studied.

Section 4: Conclusion

We have developed a simple model of an emission tomograph and derived a general covariance estimate for the number of events in bins and regions

of interest, incorporating corrections for dead time, detector sensitivity, and attenuation. The dead time correction and covariance estimates have been verified experimentally on the Donner 280-Crystal Positron Tomograph. The experiments demonstrate the importance of dead time correction at modest count rates, and the strong dependence of the covariance of the actual number of events in regions on the dead time correction factor. The covariance estimate is the link between the amount of activity administered and the covariances of the parameters to be determined in an experiment. A major conclusion from this theoretical work, verified by experiment, is that in situations with high activity in the tomograph, the covariance of the corrected data will be greater than predicted from a naive estimate based on Poisson statistics for corrected data.

Acknowledgments

The authors are grateful to T.F. Budinger and S.E. Derenzo for thoughtful criticism during the preparation of this paper. We are also indebted to Y. Yano, who provided the radionuclides, and J.A. Twitchell for technical assistance. B.M. Mazoyer is visiting from the Biophysics Department of the X. Bichat School of Medicine, Paris 7 University, and acknowledges the support of Institut National de la Recherche en Informatique et Automatique (INRIA) and Philippe Foundation, Inc. M.S. Roos is supported by NRSA training grant HL07367 from the National Institutes of Health. This work was supported in part by the Director, Office of Energy Research, Office of Health and Environmental Research of the US Department of Energy under contract No DE-AC03-76SF00098 and in part by Public Health Service Grant No HL25840 awarded by the National Heart Lung and Blood Institute, Department of Health and Human Services.

Appendix : Derivation of covariance formula

Recall from section 1 that q^e_k and q^t_k were defined as the emission and transmission datasets and p_k the corrected number of events in the kth bin as:

$$p_k = f^e q^e_k \frac{T^t}{f^t q^t_k} H_k \quad , \tag{1}$$

where T^t is the acquisition period of the transmission data, f^e and f^t the dead time correction factors for the emission and transmission datasets. Equation (1) states that p_k is a function of all of the n^x_k and m^x_k through the dead time correction factors f^x and the q^x_k. Since f^x is an implicit function of the total observed count rate $G^x = (N^x + M^x)/T^x$, we can define a function $f^{x\prime}$ as:

$$f^{x\prime} = \frac{\partial f^x}{\partial G^x} = T^x \frac{\partial f^x}{\partial n^x_k} = T^x \frac{\partial f^x}{\partial m^x_k} \quad , \tag{20}$$

for all k. For the model of Section 1:

$$f^x = \exp(\tau\, f^x G^x) \tag{21}$$

$$f^{x\prime} = \tau\, f^x (f^x + G^x f^{x\prime}) = \frac{\tau\, (f^x)^2}{1 - \tau\, f^x G^x} \quad . \tag{22}$$

We can further remark that since $q^x_j = n^x_j - m^x_j$, then:

$$\frac{\partial q^x_j}{\partial n^y_k} = \delta_{x,y}\, \delta_{j,k} \quad , \quad \frac{\partial q^x_j}{\partial m^y_k} = -\, \delta_{x,y}\, \delta_{j,k} \; . \tag{23}$$

Using logarithmic derivatives in (1), the partial derivatives of p_j are:

$$\begin{aligned}
\frac{\partial p_j}{\partial n_i^e} &= p_j \left(\frac{\delta_{i,j}}{q_j^e} + \frac{f^{e\prime}}{f^e T^e} \right) , \\
\frac{\partial p_j}{\partial m_i^e} &= p_j \left(- \frac{\delta_{i,j}}{q_j^e} + \frac{f^{e\prime}}{f^e T^e} \right) , \\
\frac{\partial p_j}{\partial n_i^t} &= -p_j \left(\frac{\delta_{i,j}}{q_j^t} + \frac{f^{t\prime}}{f^t T^t} \right) , \\
\frac{\partial p_j}{\partial m_i^t} &= -p_j \left(- \frac{\delta_{i,j}}{q_j^t} + \frac{f^{t\prime}}{f^t T^t} \right) .
\end{aligned} \tag{24}$$

Using these derivatives, each term of the double sum in the right side of equation (10) of section 2 may be computed. According to previous assumptions, $\mathrm{var}(n^x{}_i) = n^x{}_i$ and $\mathrm{var}(m^x{}_i) = m^x{}_i$; then the generic term of this sum becomes:

$$p_j p_k \left[\delta_{i,j}\delta_{i,k} \left(\frac{n_i^x + m_i^x}{q_j^x\, q_k^x}\right) + \left(\frac{f^{x\prime}}{f^x T^x}\right)^2 (n_i^x + m_i^x) + \frac{f^{x\prime}}{f^x T^x} \left(\frac{\delta_{i,j}}{q_j^x} + \frac{\delta_{i,k}}{q_k^x}\right)(n_i^x - m_i^x) \right]$$

The first term in the brackets is null unless i=j=k, and then the sum over i of these terms may be written:

$$\delta_{j,k} Q_k = \delta_{j,k} \frac{n_k^x + m_k^x}{(q_k^x)^2} \tag{25}$$

The sum over i of the second term is easily computed as a constant (independent of j and k) times the total number of counts $N^x + M^x$; due to Kronecker functions, only two terms remain when summing the third terms, one when i=j, the other when i=k. Since $q^x{}_j = n^x{}_j - m^x{}_j$, this partial sum reduces to twice $f^{x\prime}/(f^x T^x)$ (independent of j and k).

Defining as in section 2 the sum over i of the last two terms as:

$$F^x = \frac{2\ f^{x'} f^x T^x + (f^{x'})^2 (N^x + M^x)}{(f^x T^x)^2} \quad , \tag{26}$$

and Q_k and P as the sum over x of $Q^x{}_k$ and F^x respectively, equation (10) becomes:

$$\mathrm{cov}(p_j, p_k) = p_j p_k \left(\delta_{j,k} Q_k + P \right) \quad . \tag{11}$$

References

Adams R, Zimmerman D 1973 J. Nucl. Med. **14** 496-8

Arnold J E, Johnston A S, Pinsky S M 1974 J. Nucl. Med. **15** 412-6

Budinger T F 1973 in Medical Radioisotopes Scintigraphy 1972 Vol.I, STI/PUB/315 (Vienna: IAEA) pp. 501-55

Budinger T F, Huesman R H, Knittel B L, Twitchell J A, Brennan K M, Yano Y 1984 J. Nucl. Med. **25** p 69

Derenzo S E, Budinger T F, Huesman R H, Cahoon J L, Vuletich T 1981 IEEE Trans. Nucl. Sci. **NS-28:1** 81-9

Evans R D 1955 The Atomic Nucleus (New York: McGraw-Hill)

Hoffman E J, Phelps E M, Huang S C 1983 J. Nucl. Med. **24** 245-57

Huesman R H, Cahoon J 1980 IEEE Trans. Nucl. Sci. **NS-27:1** 474-8

Huesman R H 1984 Phys. Med. Biol. **29** 543-52

Marquardt D W 1963 SIAM **11** 431-41

Muehllehner G, Jaszczak R J, Beck R N 1974 Phys. Med. Biol. **19** 504-10

Sorenson J A 1975 J. Nucl. Med. **16** 284-8

Figure 1. Data from ^{82}Rb dead time experiment: (o) events in coincidence window; (*) events in no-coincidence window; (●) total number of events. a) Source without scattering material. b) Source with scattering material.

Figure 2. Data and fitted curves for ^{82}Rb experiments: (o) events in coincidence window ; (*) events in no-coincidence window; (solid lines) fits. The fits were performed for total observed count rate < 200,000 events/sec. a) Source without scattering material. b) Source with scattering material.

Figure 3. a) Correction factors computed using dead time estimates from the ^{82}Rb experiments with and without scattering material (solid and dashed line, respectively) as a function of the total observed count rate. b) Correction factors from the ^{68}Ge-^{18}FDG experiment (o) and the model with a dead time = 1.8 μsec/event (solid line).

Figure 4. a) Transmission image of phantoms. b) Emission image with regions of interest: 1- ^{68}Ge source, 2- background, 3- ^{18}FDG source, 4- patient port.

Figure 5. Counting statistics at different times during ^{68}Ge-^{18}FDG experiment. Sample mean and variance for on-time events (o and ●, respectively) and off-time events (* and ∇, respectively). This figure supports the assumption of Poisson noise for on-time and off-time events in the practical range of interest. (right of the dashed line)

Figure 6. Statistics for corrected number of events, A, as a function of the total observed count rate. a) Sample mean (*) and variance (o); predicted variance (solid line) using equation (15). b) Predicted coefficient of variation.

Figure 7. Predicted vs. observed variance of the number of events at three different total observed count rates in three regions. (^{68}Ge (o), background (●), ^{18}FDG (∇))

Figure 8. Input (a) and residue (b) curves from an $H_2{}^{15}O$ dynamic study with (●) and without (o) correction for dead time. Using the microsphere technique, the flow value (ml\min\g tissue) was measured to be 1.47; the flow values derived from the $H_2{}^{15}O$ experiment were 1.83 before and 1.39 after correction for dead time. The correction factor at the time of the peak of the input curve was 1.8 for a 180,000 events/sec total observed count rate.

Table 1. Comparison of observed and predicted covariances and correlations of number of events in two pairs of regions for ^{68}Ge-^{18}FDG experiment at three different count rates, with and without dead time correction. (see Figure 4b for regions)

Regions	Observed rate (10^3events/sec)	Covariance (correlation)		
		observed	predicted with correction	predicted without correction
1,4	40	4.27×10^3 (.14)	4.60×10^3 (.16)	3.16×10^3 (.14)
	90	5.00×10^3 (.06)	7.15×10^3 (.09)	2.94×10^3 (.07)
	180	7.25×10^4 (.13)	3.98×10^4 (.08)	2.33×10^3 (.03)
3,4	40	7.85×10^4 (.86)	8.64×10^4 (.85)	6.21×10^4 (.86)
	90	3.56×10^5 (.90)	3.18×10^5 (.90)	1.44×10^5 (.86)
	180	5.30×10^6 (.96)	3.92×10^6 (.95)	2.82×10^5 (.83)

Table 2. Statistics for prediction of number of events in three regions (see Figure 4b) at three different count rates. The two columns at the right are the contributions to the total variance (in %) of the additional variance due to the correlation between corrected number of events in different bins introduced by the correction process and the simple multiplicative effect of the correction factor. These correspond to the first and second term of equation (15), respectively.

Region #	Total observed rate (10^3events/sec)	R_a in region	Variance	eq. 15 1st term (%)	eq. 15 2nd term (%)
Background	40	6.07×10^{1}	8.16×10^{3}	0.0	100.0
2	90	1.39×10^{2}	1.65×10^{4}	0.0	100.0
	180	3.04×10^{2}	5.80×10^{4}	0.0	100.0
Low source	40	3.25×10^{3}	7.88×10^{3}	0.6	99.4
strength	90	3.27×10^{3}	1.99×10^{4}	0.4	99.6
1	180	3.59×10^{3}	7.93×10^{4}	0.6	99.4
High source	40	4.76×10^{4}	9.75×10^{4}	10.5	89.5
strength	90	1.22×10^{5}	3.48×10^{5}	26.3	73.7
3	180	3.34×10^{5}	3.86×10^{6}	72.3	27.7

Figure 1a

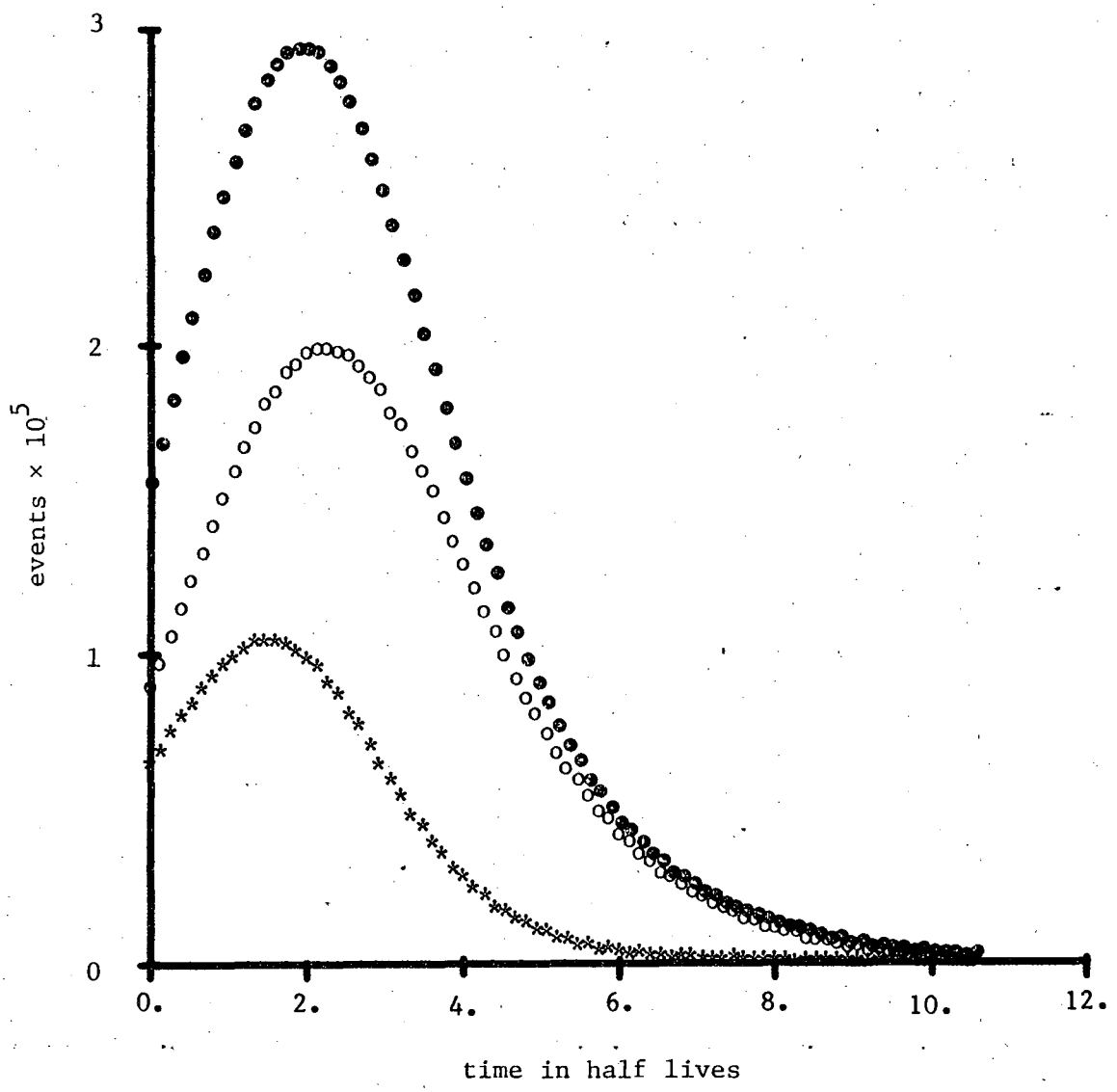

Figure 1b

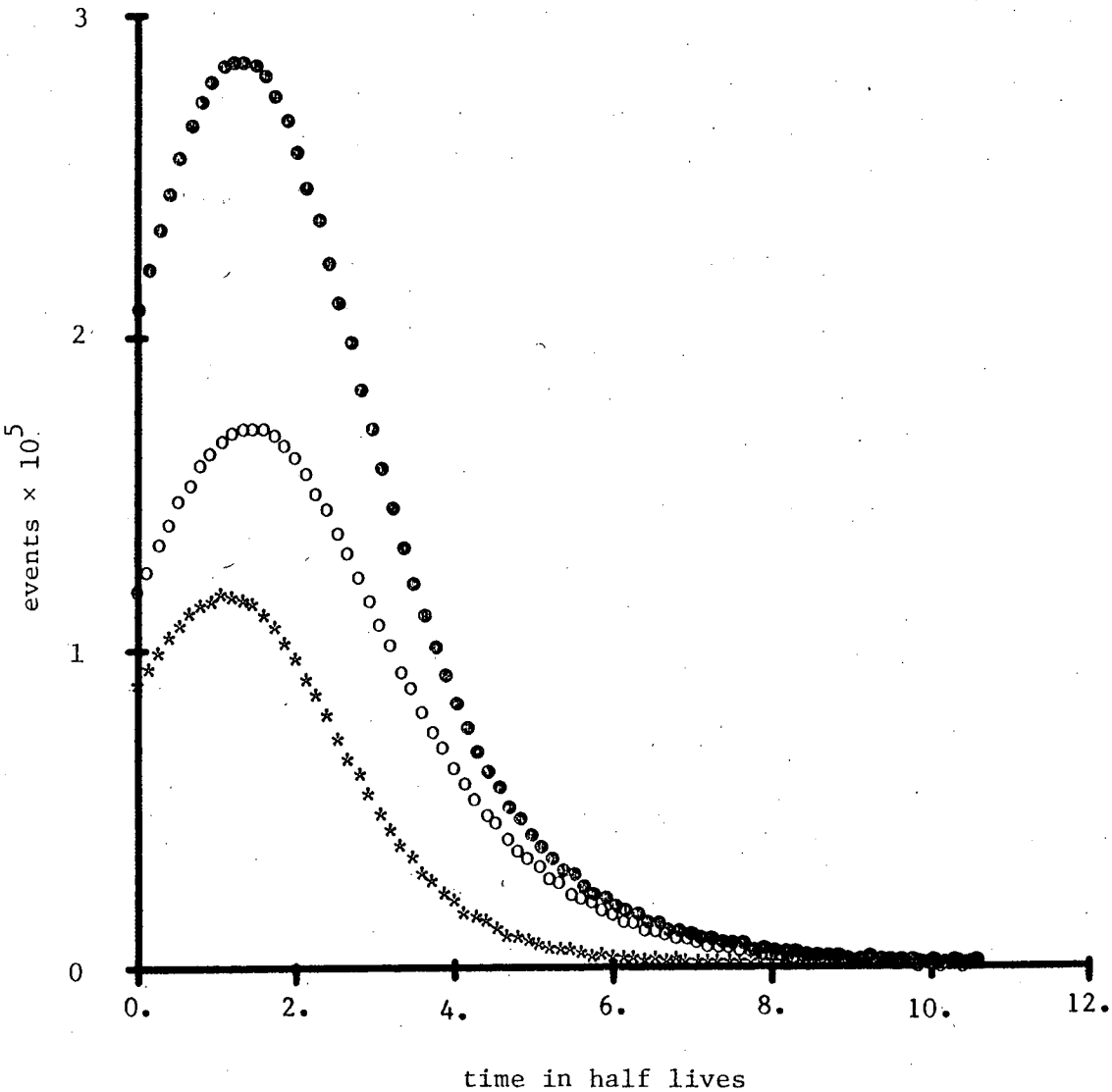

Figure 2a

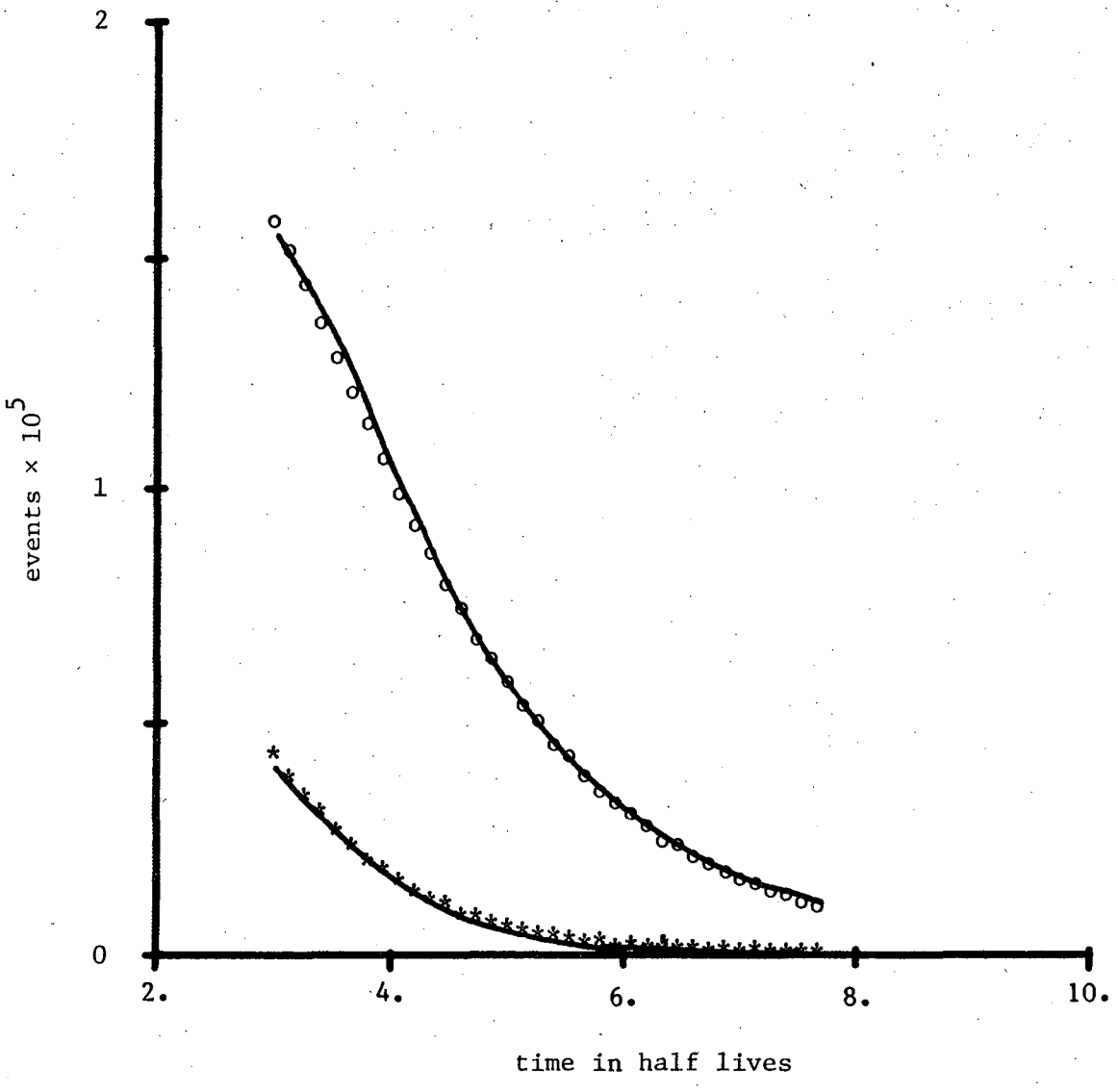

XBL 846-7181

Figure 2b

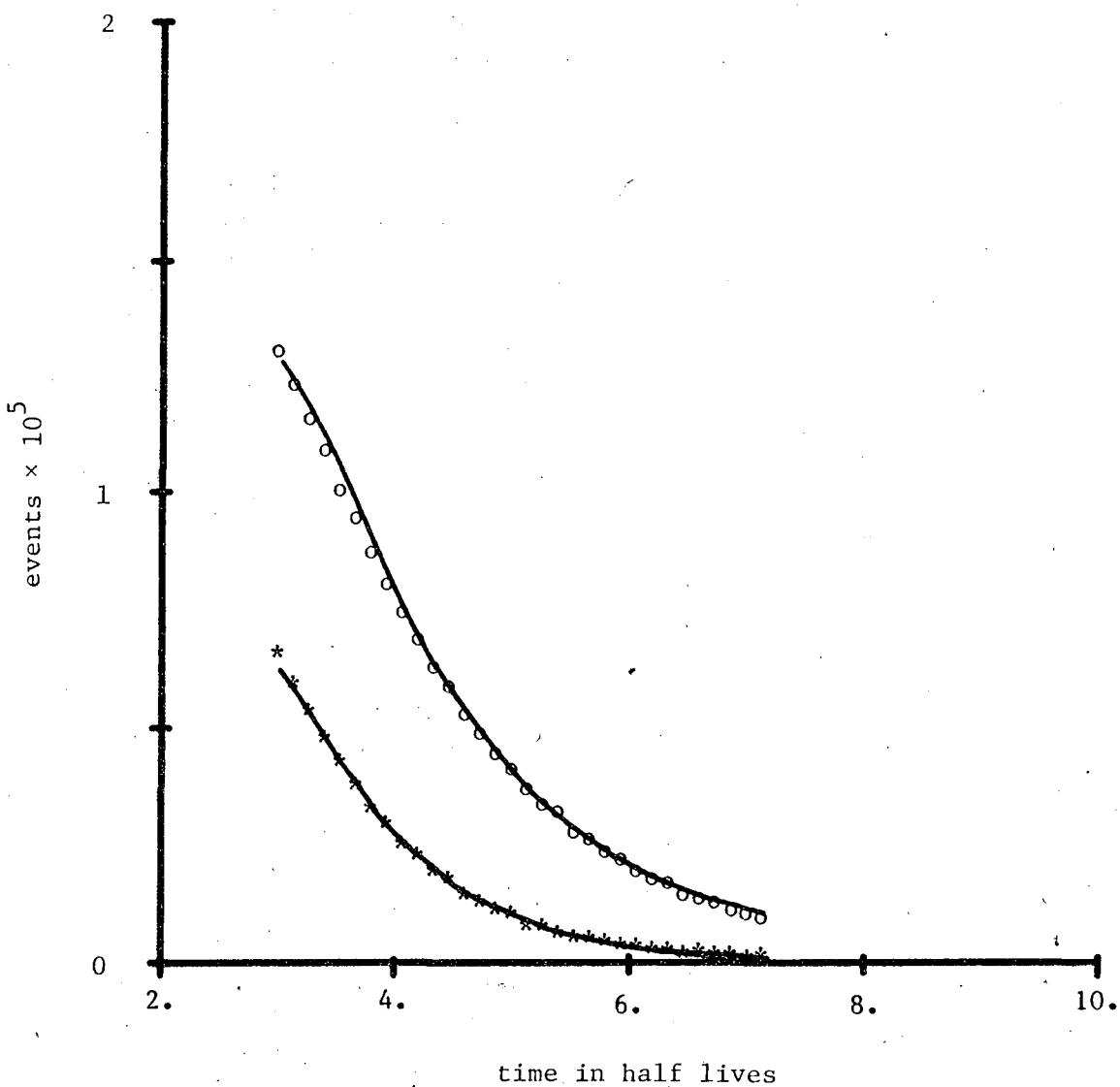

XBL 846-7183

Figure 3a

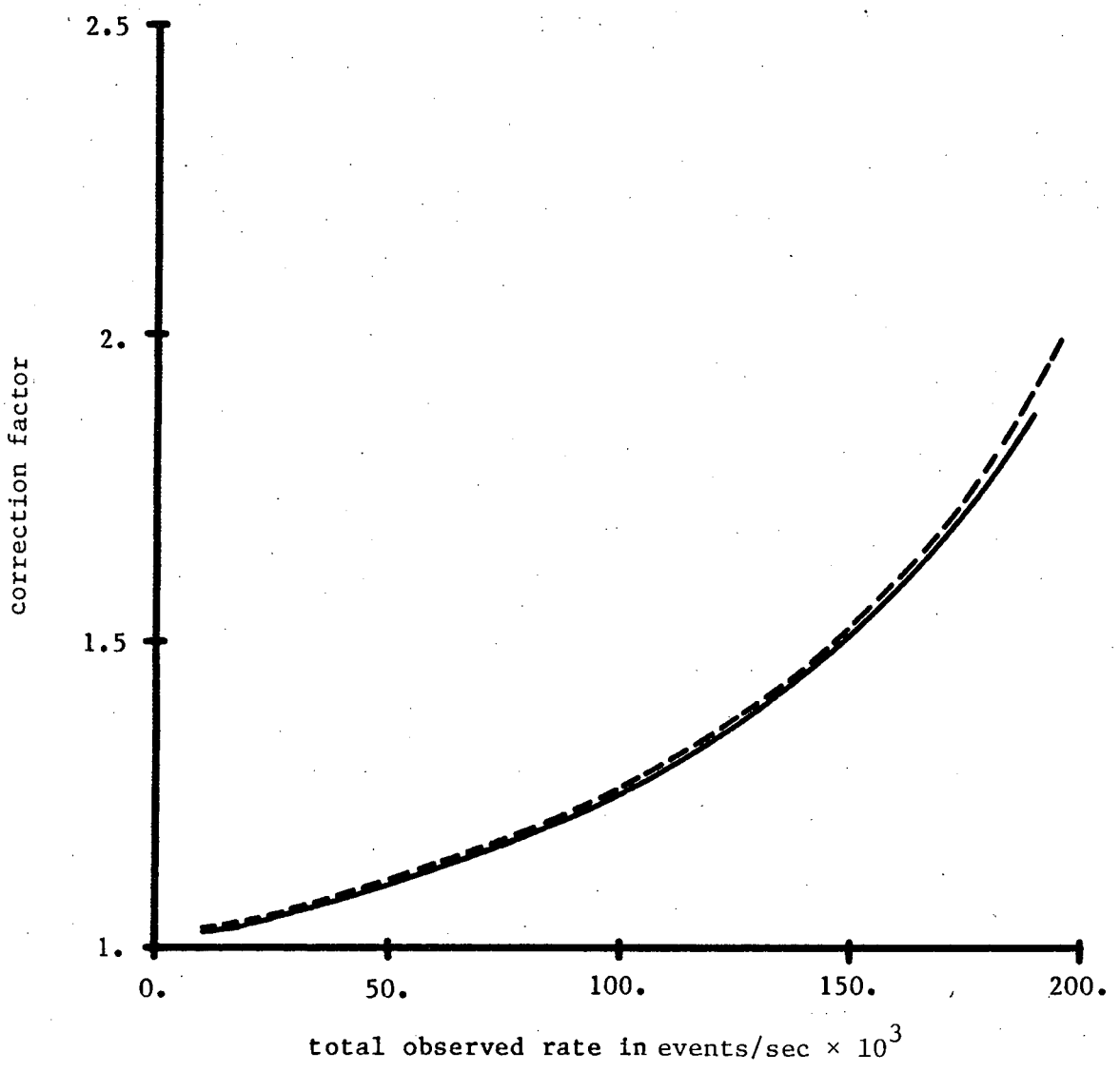

XBL 846-7185

Figure 3b

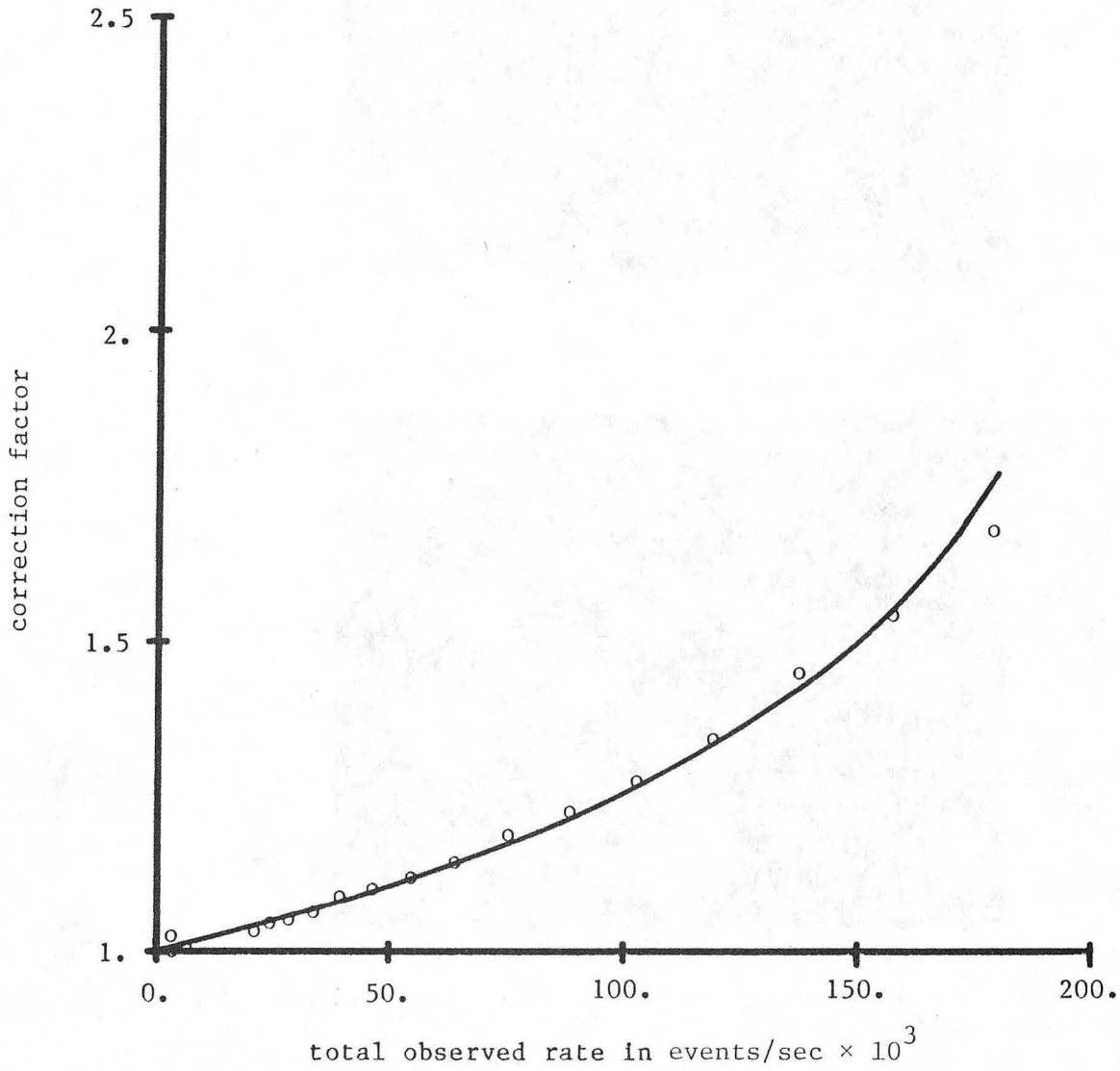

XBL 846-7189

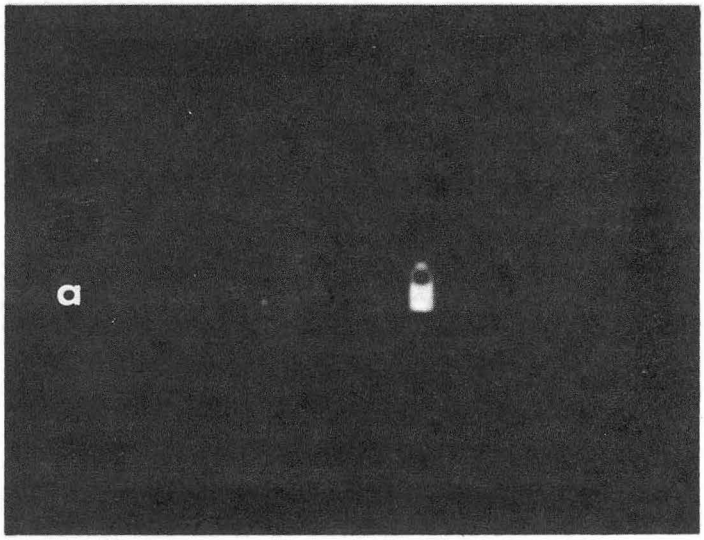
a

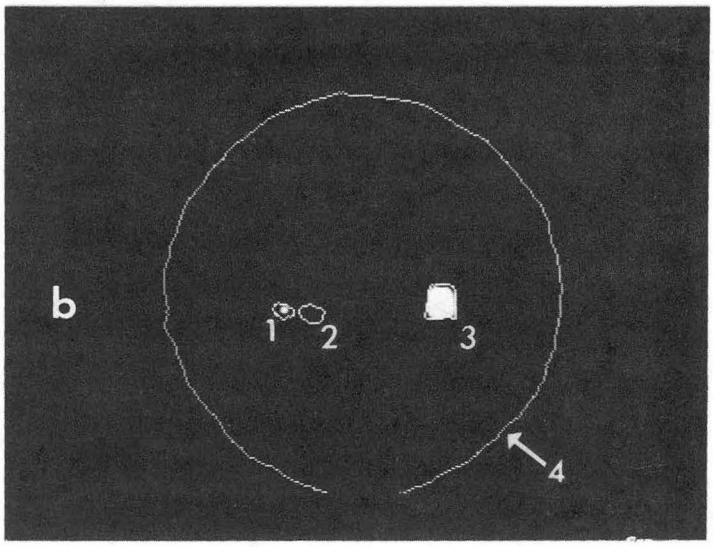
b
1
2
3
4

Figure 5

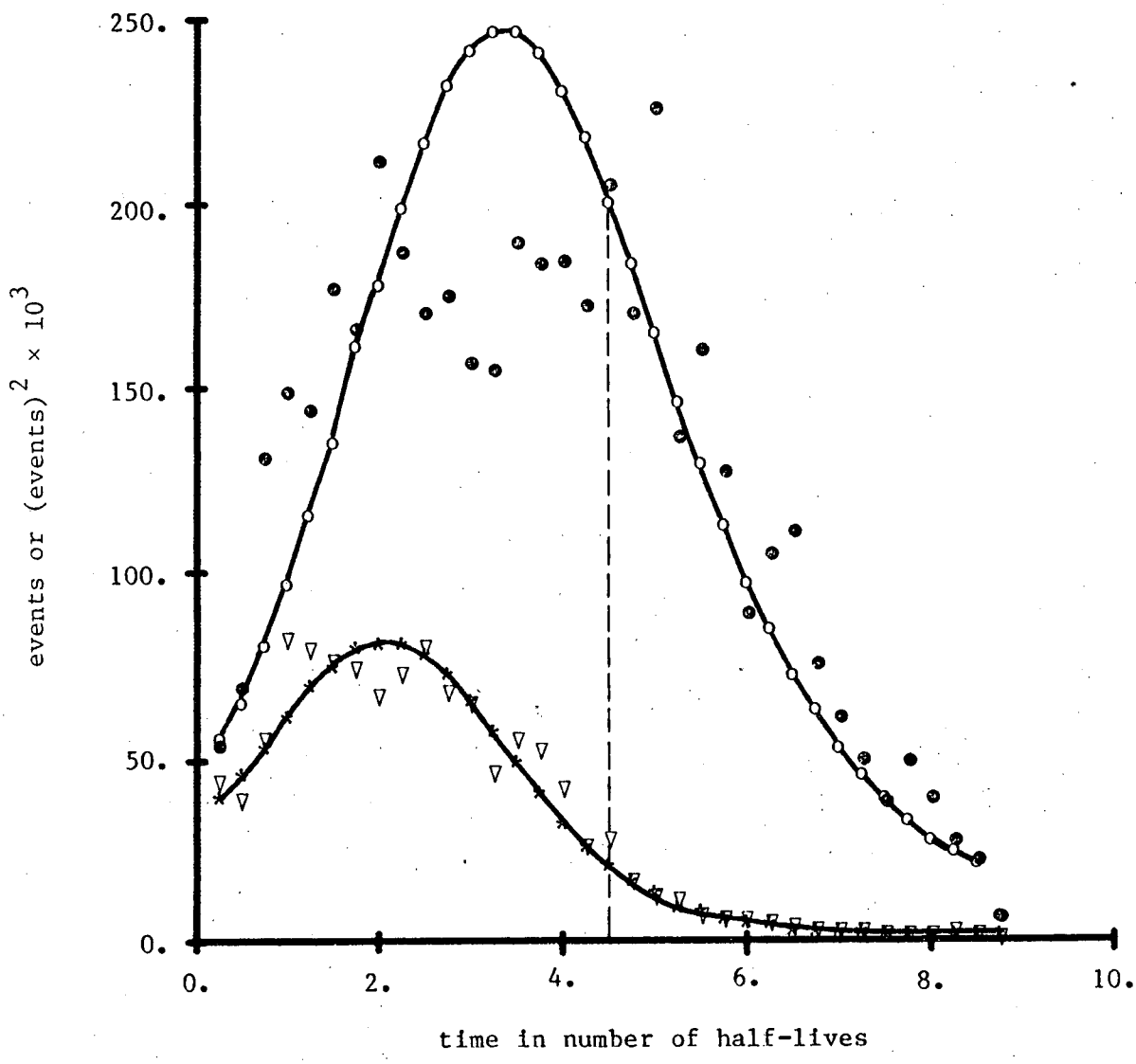

XBL 846-7179

Figure 6a

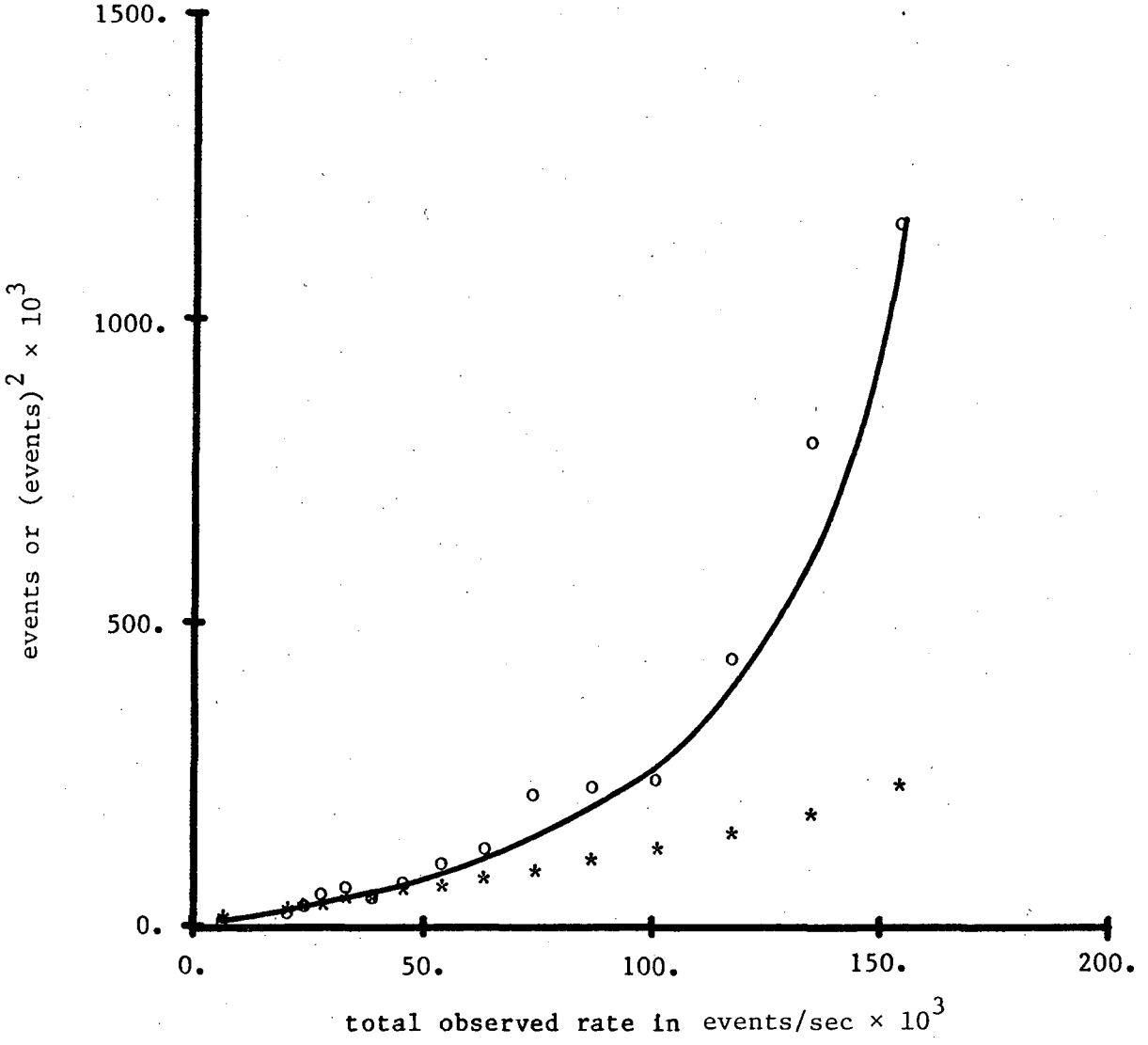

XBL 846-7191

Figure 6b

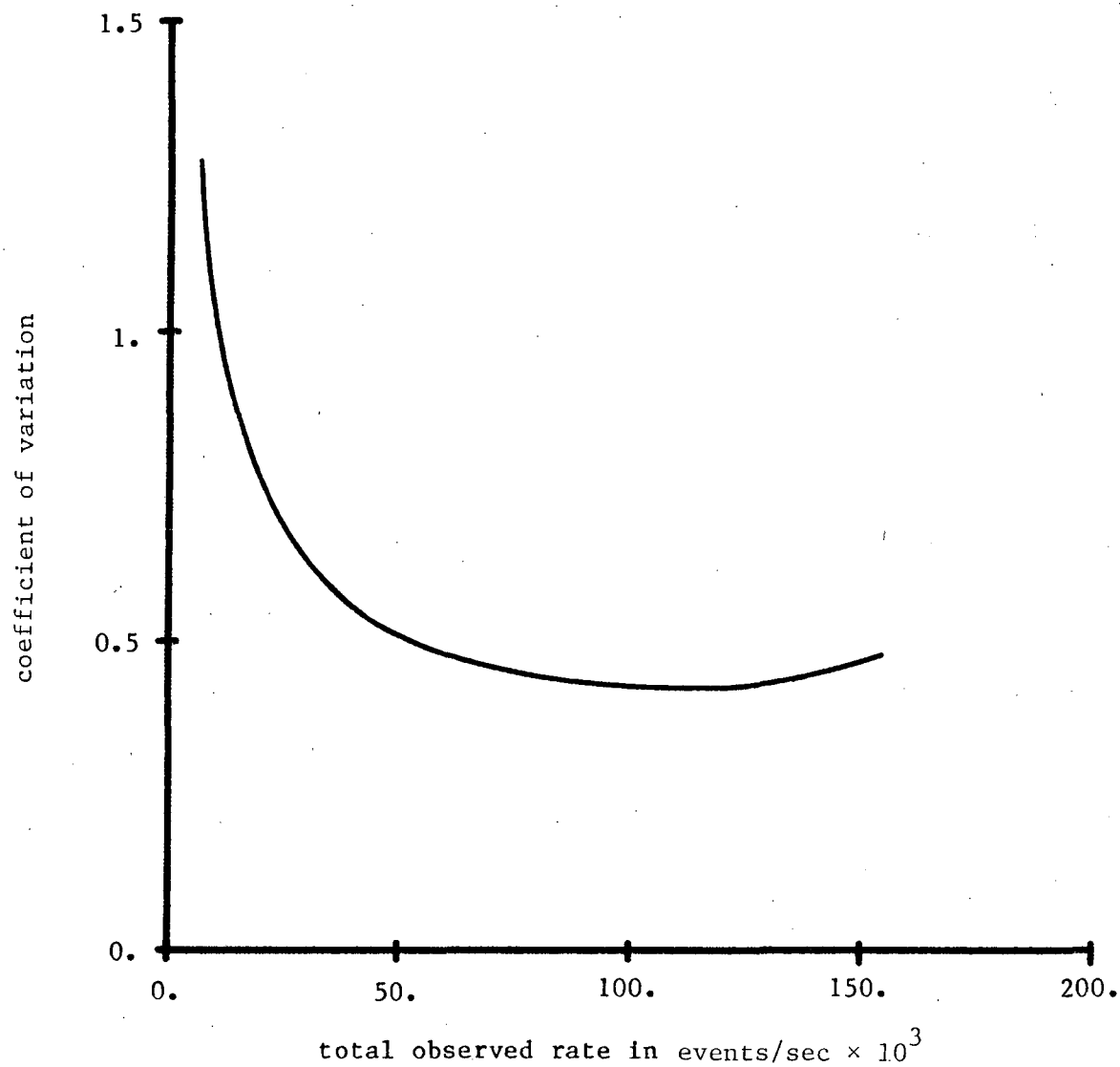

XBL 846-7187

Figure 7

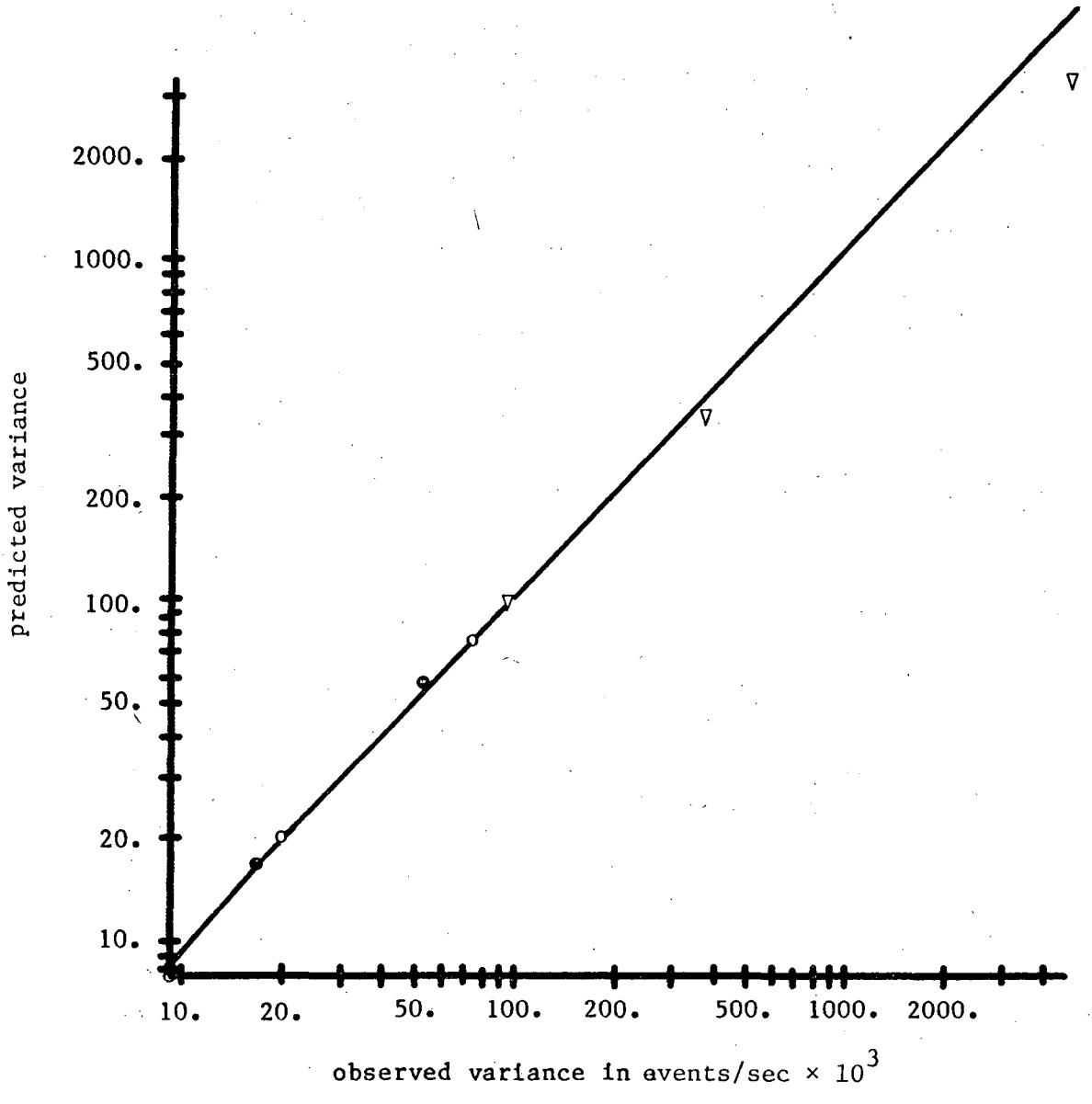

XBL 846-7193

Figure 8a

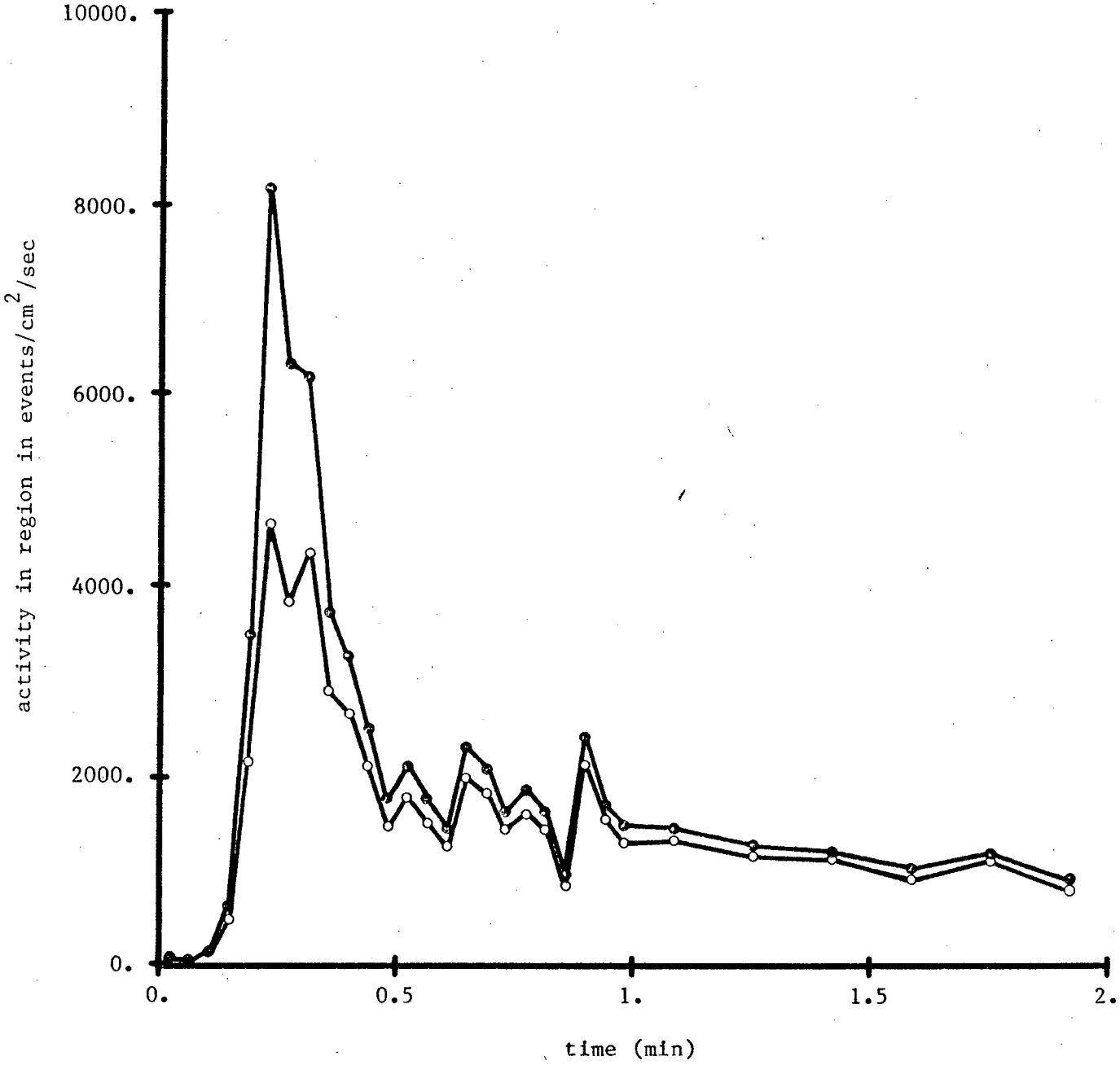

XBL 846-7197

Figure 8b

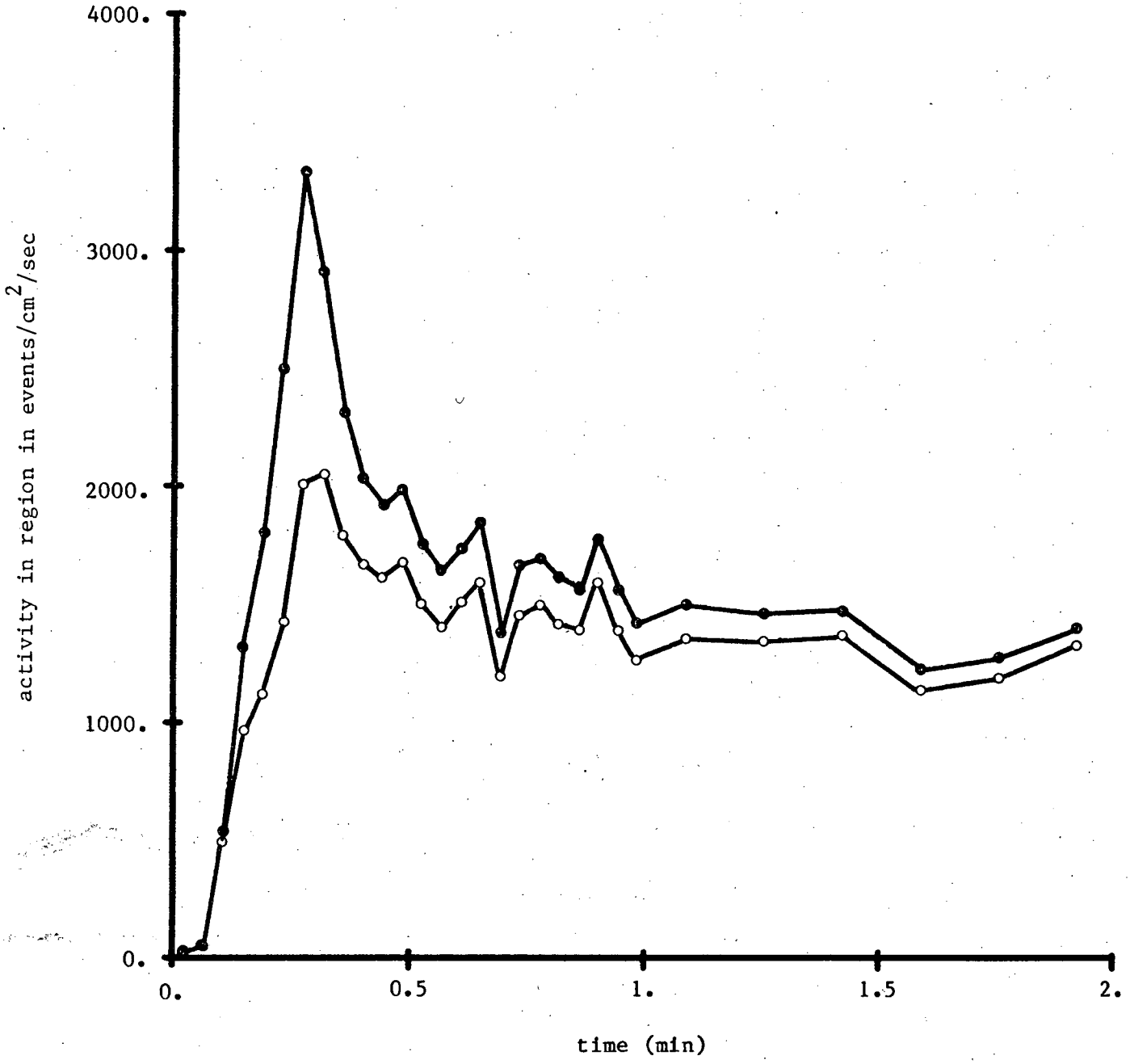

XBL 846-7195

Résumé

Correction de temps-mort et statistiques de comptage pour la tomographie à positrons.

Les auteurs présentent une correction pour les pertes de comptage dues aux temps-morts dans les études dynamiques utilisant un tomographe à positrons. Un unique temps-mort paralysant permet de modéliser la réponse du tomographe pour les taux d'évènements (evt) rencontrés en routine. Le tomographe à 280 cristaux du Donner Laboratory est ainsi caracterisé par un temps-mort de 1.8 µsec/evt pour des taux inférieurs à 200,000 evt/sec. A 180,000evt/sec le facteur de correction vaut 1.8. Cette correction est effectuée sur le nombre d'évènements de chaque projection et de chaque région d'intérêt pour toutes les images d'une étude dynamique, et la covariance des données corrigées est calculée. Pour un taux global de 180,000 evt/sec, la variance du nombre d'annihilations (après correction) dans une région en contenant 3.3×10^5 est de 3.9×10^6, 10 fois supérieure a la valeur prédite a l'aide d'un simple modèle Poissonien. Ces résultats statistiques ont ete vérifiés experimentalement. La necessité et l'importance de cette correction de temps-mort dans les études dynamiques utilisant la tomographie à positrons est mise en évidence dans un exemple ou l'absence de correction entraine une surestimation de 25% de la perfusion du myocarde.

This report was done with support from the Department of Energy. Any conclusions or opinions expressed in this report represent solely those of the author(s) and not necessarily those of The Regents of the University of California, the Lawrence Berkeley Laboratory or the Department of Energy.

Reference to a company or product name does not imply approval or recommendation of the product by the University of California or the U.S. Department of Energy to the exclusion of others that may be suitable.

TECHNICAL INFORMATION DEPARTMENT
LAWRENCE BERKELEY LABORATORY
UNIVERSITY OF CALIFORNIA
BERKELEY, CALIFORNIA 94720